EPA/600/A-93/253

Measurements of Soil Permeability and Pressure Fields in EPA's Soil-gas Chamber

by: Ronald B. Mosley
U.S. Environmental Protection Agency
Air and Energy Engineering Research Laboratory
Research Triangle Park, NC 27711

Richard Snoddy and
Samuel A. Brubaker, Jr.
Acurex Environmental Corp.
P.O. Box 13109
Research Triangle Park, NC 27709

ABSTRACT

EPA's soil-gas chamber was designed to study the production and transport of radon and other potential indoor air pollutants originating in soils. This chamber is instrumented to measure distributions of radon and pressure fields. It is also instrumented to measure moisture distributions and their resulting influence on soil permeability. An analytic solution for advective flow in the soil-gas chamber is presented which includes the effects of moisture-dependent spatial variations of the permeability. Measurements of the pressure field are compared with the model calculations. Relatively good agreement between the measurements and calculations is obtained except in the region near the water level where the boundary conditions are not rigorously satisfied.

This paper has been reviewed in accordance with the U.S. Environmental Protection Agency's peer and administrative review policies and approved for presentation and publication.

Introduction

In an effort to better understand the mechanisms of transport and entry of radon and other soil contaminants into the indoor air environment, EPA has constructed and instrumented a soil chamber to simulate and study these mechanisms. This paper will report some early results from these studies. This facility has been discussed elsewhere (1) and will not be described in detail here. Because it is believed that advective transport is usually the dominant mechanism for pollutant entry into indoor air (2-9), this paper will concentrate on the advective aspects of radon transport. It will first present a model using analytic solutions to describe the advective flow including the effects of moisture dependent permeability. Preliminary measurements will also be compared to the model predictions.

Some developments presented in three previous papers (10-12) will be combined to derive a solution to the advective transport equation that is applicable to the soil research chamber at EPA's Air and Energy Engineering Research Laboratory (AEERL). Reference (10) presented an analytic solution for advective flow of soil gas into an infinitely long porous cylinder buried parallel to the surface of the soil. The physical properties of the soil, including the permeability, were assumed to be uniform and isotropic. Reference (11) modified the model from reference (10) to account for the effects of moisture variation with depth on the permeability of the soil. Reference (12) modified the solution for the semi-infinite block of soil with uniform permeability to satisfy the boundary conditions at the vertical walls of the research chamber at AEERL. This paper combines these three methods of solution to yield an analytic solution for pressures and flows that is applicable to the research chamber even when permeability varies with the moisture in the vertical direction.

Development of the Equations

The steady state flow of radon in soil gas, which is treated as incompressible in the applicable pressure range, is described by three equations:

$$\nabla \cdot \frac{k}{\mu} \nabla P = 0 \qquad (1)$$

$$\vec{v} = -\frac{k}{\mu} \nabla P \qquad (2)$$

$$\nabla \cdot D_e \nabla C - \frac{\vec{v}}{\epsilon} \cdot \nabla C - \lambda C + G = 0. \quad (3)$$

Equation (1) is the continuity equation, equation (2) is Darcy's law, and equation (3) represents the diffusion, advection, decay, and generation of radon in the soil gas. A solution to equation (1) can be obtained (10) for the case in which the permeability and gas viscosity are independent of position. However, even if the physical properties of the soil are highly uniform, the soil moisture will have a vertical distribution due to the influence of gravity. Since the permeability varies markedly with moisture content, the permeability can be expected to vary with depth in the soil. This is particularly true near a zone of saturation such as near the water table.

In order to take advantage of the previously mentioned solution, a coordinate transformation will be applied in which

$$\xi = \frac{k_0}{k(y)} x \quad (4)$$

and

$$\varphi = k_0 \int_0^y \frac{dt}{k(t)}. \quad (5)$$

This transformation is very similar to one described previously (11). The present transformation is more practical to apply because it is defined to have the same dimensions as the original system which was not the case in reference (11).

These new coordinates transform equation (1) into

$$\frac{\partial^2 P}{\partial \xi^2} + \frac{\partial^2 P}{\partial \varphi^2} = 0 \quad (6)$$

which is the same form that would have occurred for constant permeability. In applying the solution from reference (10), it is assumed that the original cylinder transforms as a cylinder in the new reference frame. This assumption, of course, is not rigorously correct, but is not a bad approximation when k(y) varies slowly in the vicinity of the cylinder. This condition will be relatively well met in the experimental chamber.

Using the above assumptions, the solution from reference (10) can be written as

$$P(\xi,\varphi)=P_c\frac{\ln\left(\frac{\xi^2+(\varphi+\sqrt{\varphi_h^2-b'^2})^2}{\xi^2+(\varphi-\sqrt{\varphi_h^2-b'^2})^2}\right)}{\ln\left(\frac{\varphi_h+\sqrt{\varphi_h^2-b'^2}}{\varphi_h+\sqrt{\varphi_h^2-b'^2}}\right)}. \tag{7}$$

This solution applies for an infinitely long cylinder in a semi-infinite block of soil in the new coordinate system. For the solution to be applicable to the soil research chamber, it not only must be transformed back to the original reference frame, but it also must be made to satisfy the boundary conditions imposed by the finite size of the experimental chamber. This latter task will be accomplished by applying the classic method of images to simulate the influences of the vertical walls of the chamber. Because flow near the bottom of the chamber will be dominated by the changing permeability, the boundary condition on velocity at the bottom surface of the chamber has not been rigorously pursued.

When the inverse transformation is carried out and an infinite number of image solutions are superposed to simulate the effects of the walls of the chamber, the resulting pressure can be written as

$$\begin{aligned}P(x,y)= \; & P'\ln\left(\frac{x^2+(\Gamma+\Phi)^2}{x^2+(\Gamma-\Phi)^2}\right)\\ & +P'\sum_1^{\infty}\ln\left(\frac{(4hi+x)^2+(\Gamma+\Phi)^2}{(4hi+x)^2+(\Gamma-\Phi)^2}\right)\\ & +P'\sum_1^{\infty}\ln\left(\frac{(4hi-x)^2+(\Gamma+\Phi)^2}{(4hi-x)^2+(\Gamma-\Phi)^2}\right)\end{aligned} \tag{8}$$

where

$$P'=P_c\left[\ln\left(\frac{I(h)+\sqrt{I^2(h)-b'^2}}{I(h)-\sqrt{I^2(h)-b'^2}}\right)+2\left(\frac{I(h)}{4h}\,\frac{k(h)}{k_0}\right)^2\zeta(2)\right]^{-1} \tag{9}$$

and $\zeta(2)=1.64$. The flow streamlines are given by

$$\psi(x,y) = \frac{\psi_0}{\pi}\left[\tan^{-1}\left(\frac{\Gamma+\Phi}{x}\right)-\tan^{-1}\left(\frac{\Gamma-\Phi}{x}\right)\right] + \frac{\psi_0}{\pi}\sum_1^{\infty}\left[\tan^{-1}\left(\frac{\Gamma+\Phi}{4hi+x}\right)-\tan^{-1}\left(\frac{\Gamma-\Phi}{4hi+x}\right)\right] - \frac{\psi_0}{\pi}\sum_1^{\infty}\left[\tan^{-1}\left(\frac{\Gamma+\Phi}{4hi-x}\right)-\tan^{-1}\left(\frac{\Gamma-\Phi}{4hi-x}\right)\right]. \quad (10)$$

The components of velocity can be obtained by differentiating either equation (8) or (10). The horizontal component is given by

$$v_x(x,y) = \frac{8P'k_0\Phi}{\mu}\left\{\frac{x\Gamma}{[x^2+(\Gamma+\Phi)^2][x^2+(\Gamma-\Phi)^2]} + \sum_1^{\infty}\frac{(4hi+x)\Gamma}{[(4hi+x)^2+(\Gamma+\Phi)^2][(4hi+x)^2+(\Gamma-\Phi)^2]} + \sum_1^{\infty}\frac{(4hi-x)\Gamma}{[(4hi-x)^2+(\Gamma+\Phi)^2][(4hi-x)^2+(\Gamma-\Phi)^2]}\right\} \quad (11)$$

and the vertical component is given by

$$v_y(x,y) = \frac{-4P'k_0\Phi}{\mu}\left\{\frac{x^2\left[1+2\frac{k'(y)}{k(y)}\Gamma\right]+\Phi^2-\Gamma^2}{[x^2+(\Gamma+\Phi)^2][x^2+(\Gamma-\Phi)^2]} + \sum_1^{\infty}\frac{(4hi+x)^2\left[1+2\frac{k'(y)}{k(y)}\Gamma\right]+\Phi^2-\Gamma^2}{[(4hi+x)^2+(\Gamma+\Phi)^2][(4hi+x)^2+(\Gamma-\Phi)^2]} + \sum_1^{\infty}\frac{(4hi-x)^2\left[1+2\frac{k'(y)}{k(y)}\Gamma\right]+\Phi^2-\Gamma^2}{[(4hi-x)^2+(\Gamma+\Phi)^2][(4hi-x)^2+(\Gamma-\Phi)^2]}\right\}. \quad (12)$$

Upon integrating equation (12) over the soil surface, the total rate of flow is obtained as

$$Q = \frac{4\pi L k_0 P'}{\mu}. \quad (13)$$

Equation (13) provides a means of measuring k_0. However, since P' contains the ratio $k(h)/k_0$, information about the variation of permeability with depth is required. Using a measured moisture profile, an empirical model by Rogers and Nielsen (13) can be used to calculate the permeability. This empirical model relates the permeability to the moisture content as

$$k=k_0\exp(-12s^4). \tag{14}$$

When s, the fraction of moisture saturation, is measured as a function of depth in the soil, the vertical permeability profile can be computed. Knowing the moisture content at depth h allows the ratio $k(h)/k_0$ to be evaluated as

$$\frac{k(h)}{k_0}=\exp[-12s^4(h)]. \tag{15}$$

Equations (9) and (13) can then be solved for the permeability at the surface of the soil as

$$k_0=\frac{Q\mu}{4\pi LP_c}\left[\ln\left(\frac{I(h)+\sqrt{I^2(h)-b'^2}}{I(h)-\sqrt{I^2(h)-b'^2}}\right)+\frac{\zeta(2)}{8}\frac{I^2(h)}{h^2}\exp(-24s^4)\right]. \tag{16}$$

Moisture and Permeability Measurements

Soil moisture was measured with a Troxler Sentry 200-AP moisture monitor. This device consists of a sensor which moves vertically inside a hollow polyvinyl chloride (PVC) tube in the soil. It measures the percent water by volume in the soil to an accuracy of 0.2% by measuring the effective capacitance of the surrounding soil. Moisture measurements were taken 0.15 m apart at four different locations within the chamber.

The measured moisture profiles are illustrated in Fig. 1. Note that the moisture approaches zero near the surface where evaporation occurs. From about 0.4 m to 1.2 m the moisture remains nearly constant at about 15% of saturation. At depths greater than 1.2 m, the moisture increases rapidly to saturation at about 1.9 m which is near the water level.

The permeability as computed from the empirical model of Rogers and Nielsen is shown in Fig. 2 This figure illustrates that the permeability is relatively independent of moisture until the level reaches about 0.2 of saturation. For levels above 0.2, the permeability decreases very rapidly with increasing moisture. An initial estimate of k_0 is given by

$$k_0=3.86x10^{-6}\epsilon^2d^{4/3} \tag{17}$$

where d is the average diameter of soil particles that pass through a No. 4 mesh screen. For the present soil, d = $3.8x10^{-4}$ m. This estimate was used to compute the profiles shown in Fig. 2. The permeability profile as a function of depth is then used to evaluate the transformation in equations (4) and (5) as well as to compute I(h) in equation (9). A more rigorous value of k_0 can be obtained from equation (16). More appropriately, linear regression is applied to the measured flow/pressure relationship and the

resulting slope used to compute k_0 from

$$k_0 = \frac{\mu}{4\pi L}\left[\ln\left(\frac{I(h)+\sqrt{I^2(h)-b'^2}}{I(h)-\sqrt{I^2(h)-b'^2}}\right)+\frac{\zeta(2)}{8}\frac{I^2(h)}{h^2}\exp\{-24s^4(h)\}\right]slope. \quad (18)$$

Figure 3 shows the flow rate as a function of the applied pressure. The slope is found to be 1.60×10^{-6} m^4 s kg^{-1}. Equation (18) then yields $k_0 = 3.17\times10^{-11}$ m^2, with $\mu = 1.85\times10^{-5}$ kg m^{-1} s^{-1}, L = 0.66 m, h = 0.965 m, b' =0.0254 m, and $\zeta(2)$ = 1.64.

Pressure Measurements

The permeability profiles in Fig. 2 are also used to compute the pressures and streamlines given by equations (8) and (10), respectively. Calculated pressure contours in the measurement plane are illustrated in Fig. 4. For a comparison, the upper portion of the figure shows the pressure contours when permeability is constant (k_0) throughout the region. The lower portion of the figure shows the pressure contours when the permeability varies as shown in Fig. 2. Significant differences in the pressure contours are apparent where the moisture content increases dramatically. The pressure differences are not effectively transmitted through regions of high moisture near the bottom of the chamber. The strong influence of moisture is perhaps even more apparent in the stream function illustrated in Fig. 5. The upper portion of the figure corresponds to the case of constant permeability, while the lower portion corresponds to variable permeability shown in Fig. 2. Note how flow is excluded from the bottom portion of the chamber where the permeability is low due to high moisture content. This result is consistent with observations in Fig. 4.

Fig. 6 shows pressure distribution in the horizontal direction at five different vertical levels. Each vertical level was chosen to correspond to a row of measurement probes in the chamber. The center row contains the suction tube located at x = 0. Note that the greatest pressure variations occur near the suction tube. As might be expected, the pressure decreases more quickly in the direction of the open surface. The symbols in this figure represent measurements of the pressure. Generally, the agreement between measurements and predictions is good. The agreement is no worse than about 14% except for certain points located in the bottom row and a few points on the extreme right side of the chamber. Certain evidence, such as frequently collecting water in the sampling lines, suggests that the soil near the right wall of the chamber may contain higher moisture contents than the rest of the soil at the same level. Consequently, the moisture profile and the resulting permeability profile near the right wall of the chamber may not correspond to those in Figs. 1 and 2 that were used

to compute the pressure. The closest moisture measurement column is located about 0.8 m from the pressure sensors at the right side. The model underpredicts the pressure somewhat near the bottom where the moisture is highest. The principal reason for this underprediction may be that the solution does not rigorously satisfy the boundary condition of zero vertical flow at the bottom surface of the chamber. This slight underprediction of the pressure in this region should have little influence on other physical quantities such as total flow rate and radon migration, since the low value of permeability in the lower region of the chamber forces the flow to go to zero at depths somewhat above the bottom surface of the chamber.

Discussion and Conclusions

A model is presented to describe advective flow in AEERL's soil-gas research chamber. The model satisfies the appropriate boundary conditions at the vertical walls of the chamber and accounts for the effects of variations in permeability with the moisture content of the soil. It was seen that the lower permeability due to moisture caused a greater fraction of the total pressure drop to occur near the central porous tube. While the model generally shows good agreement with pressure measurements, there are two regions in which some deviations occur. The model tends to overpredict the pressure at the sensor locations near the right wall of the chamber. This is the region where higher-than-normal levels of moisture were suspected. Local measurements of permeability tended to support this conclusion. The model tends to underpredict the pressure at the sensor locations near the bottom of the chamber. This is the region in which the solution is less rigorous in the sense that the condition of zero vertical flow at the surface is not imposed on the solution. For convenience, the rationale was used that, since the low values of permeability in that region would prevent any gas flow, it would not be necessary to impose a no flow condition on the solution. As was seen by the streamlines (Fig. 5), no flow occurs near the bottom of the chamber. While this lack of rigor leads to a modest error (100%) in the local pressure field, it probably has no significant effect on pollutant transport because negligible flow occurs in this region anyway. In order to confirm these assumptions, the solution will be modified in the future to satisfy the boundary conditions. If necessary, this will be done with numerical solutions.

In the present case, it is found that incorporation of the effects of moisture on permeability improves the mathematical representation of the pressure field by as much as 25%. However, sandy soils probably exhibit the least effects of the moisture profile. Moisture retention in most soils is expected to be greater than for sands. Consequently, the effect of the moisture profile is probably minimal in the present case. The moisture effects contained in this solution should take on greater significance for clay soils.

References

1. Menetrez, M.Y., Mosley, R.B., Snoddy, R., Ratanaphruks,K., and Brubaker, S.A., Jr. Evaluation of radon movement through soil and foundation substructures. Presented at the 1993 International Symposium on Measurement of Toxic and Related Air Pollutants, Durham, NC, May 4-7, 1993.
2. Bruno, R.C. Sources of indoor radon in houses: a review. JAPCA, v. 33, no. 2, pp. 105-109, 1983.
3. Nero, A.V. and Nazaroff, W.W. Characterizing the source of radon indoors. Radiat. Prot. Dosim. v. 7, pp. 23-39, 1984.
4. Nazaroff, W.W. and Doyle, S.M. Radon entry into houses having a crawl space. Health Phys., v. 48, pp. 265-281, 1985.
5. Akerblom, G., Anderson, P., and Clavenajo, B. Soil gas radon - a source of indoor radon daughters. Radiat. Prot. Dosim. v. 7, pp. 49-54, 1984.
6. Nazaroff, W.W., Feustel, H., Nero, A.V., Revzan, K.L., Grimsrud, D.T., Essling, M.A., and Toohey, R.E. Radon transport into a detached house with a basement. Atmospheric Environment, v. 19, no. 1, pp. 31-46, 1985.
7. Sextro, R.G., Moed, B.A., Nazaroff, W.W., Revzan, K.L., and Nero, A.V. Investigation of soil as a source of indoor radon. In: Radon and Its Decay Products: Occurrence, Properties, and Health Effects: Hopke, P., ed.; ACS Symposium Series 331; American Chemical Society: Washington D.C., pp. 10-29, 1987.
8. Turk, B.H., Prill, R.J., Grimsrud, D.T., Moed, B.A., and Sextro, R.G. Characterizing the occurrence, sources, and variability of radon in Pacific Northwest USA homes. J. Air Waste Manage. Assoc. v. 40, pp. 498-506, 1990.
9. Garbesi, K., Sextro, R.G., Fisk, W.J., Modera, M.P., and Revzan, K.L. Soil-gas entry into an experimental basement: model measurement comparison and seasonal effects. Eviron. Sci. Technol. v. 27, no. 3, pp. 466-473, 1993.
10. Mosley, R.B. A simple model for describing radon migration and entry into houses. In: Cross, F.T., ed., Indoor Radon and Lung Cancer: Reality or Myth?; Part 1, Battelle Press, Columbus, OH, v. 1, pp. 337-356, 1992.
11. Mosley, R.B. Model based pilot scale research facility for studying production, transport, and entry of radon into structures. In: Proceedings: the 1992 International Symposium on Radon and Radon Reduction Technology: vol. 1. EPA-600/R-93-083a (NTIS PB93-196194), pp. 6-123 thru 6-140, May 1993.
12. Mosley, R.B. An analytical solution to describe the pressure/flow relationship in EPA's soil-gas chamber. Presented at the 1993 International Symposium on Measurement of Toxic and Related Air Pollutants, Durham, NC, May 4-7, 1993.
13. Rogers, V.C. and Nielsen, K.K. Correlation of Florida soil-gas permeabilities with grain size, moisture, and porosity. EPA-600/8-91-039 (NTIS PB91-211904), June 1991.

Nomenclature

b'	$k_0\int_{h-b}^{h+b}\frac{dy}{k(y)}$, the transformed radius of the cylinder (m)
C	the activity concentration (Bq m^{-3})
d	the average diameter of soil particles that penetrate a No. 4 mesh screen (m)
D_e	the effective diffusion coefficient (m^2 s^{-1})
G	the radon generation rate (Bq m^{-3} s^{-1})
h	the depth of the cylinder (m)
i	a summation index (unitless)
I(h)	$k_0\int_0^h\frac{dy}{k(y)}$
k	k(y), the permeability of the soil (m^2)
k_0	the soil permeability at the soil surface (m^2)
k(h)	the soil permeability at the level of the cylinder (m^2)
$k'(y)$	dk/dy is the derivative of the permeability (m)
L	the length of the central section of the cylinder (m)
P	pressure (Pa)
P_c	the pressure applied at the central cylinder (Pa)
P'	a pressure coefficient (Pa)
Q	the gas flow rate (m^3 s^{-1})
s	the fraction of moisture saturation
t	an integration variable (m)
v	the superficial velocity (m s^{-1})
x	the horizontal Cartesian coordinate (m)
y	the vertical Cartesian coordinate (m)
Γ	$k(y)\int_0^y\frac{dt}{k(y)}$
ϵ	the soil porosity (unitless)
ζ	the Riemann zeta function
λ	the decay constant for radon (s^{-1})
μ	the viscosity of the soil gas (kg m^{-1} s^{-1})
ξ	the transformation coordinate corresponding to x (m)
Φ	$\frac{k(y)}{k_0}\sqrt{\varphi_h^2-b'^2}$
φ	the transformation coordinate corresponding to y (m)
φ_h	$k_0\int_0^h\frac{dt}{k(y)}$, the transformed depth of the cylinder (m)
ψ	the stream function (m^2 s^{-1})
ψ_0	the stream function evaluated at the origin (m^2 s^{-1})
∂	the partial derivative symbol

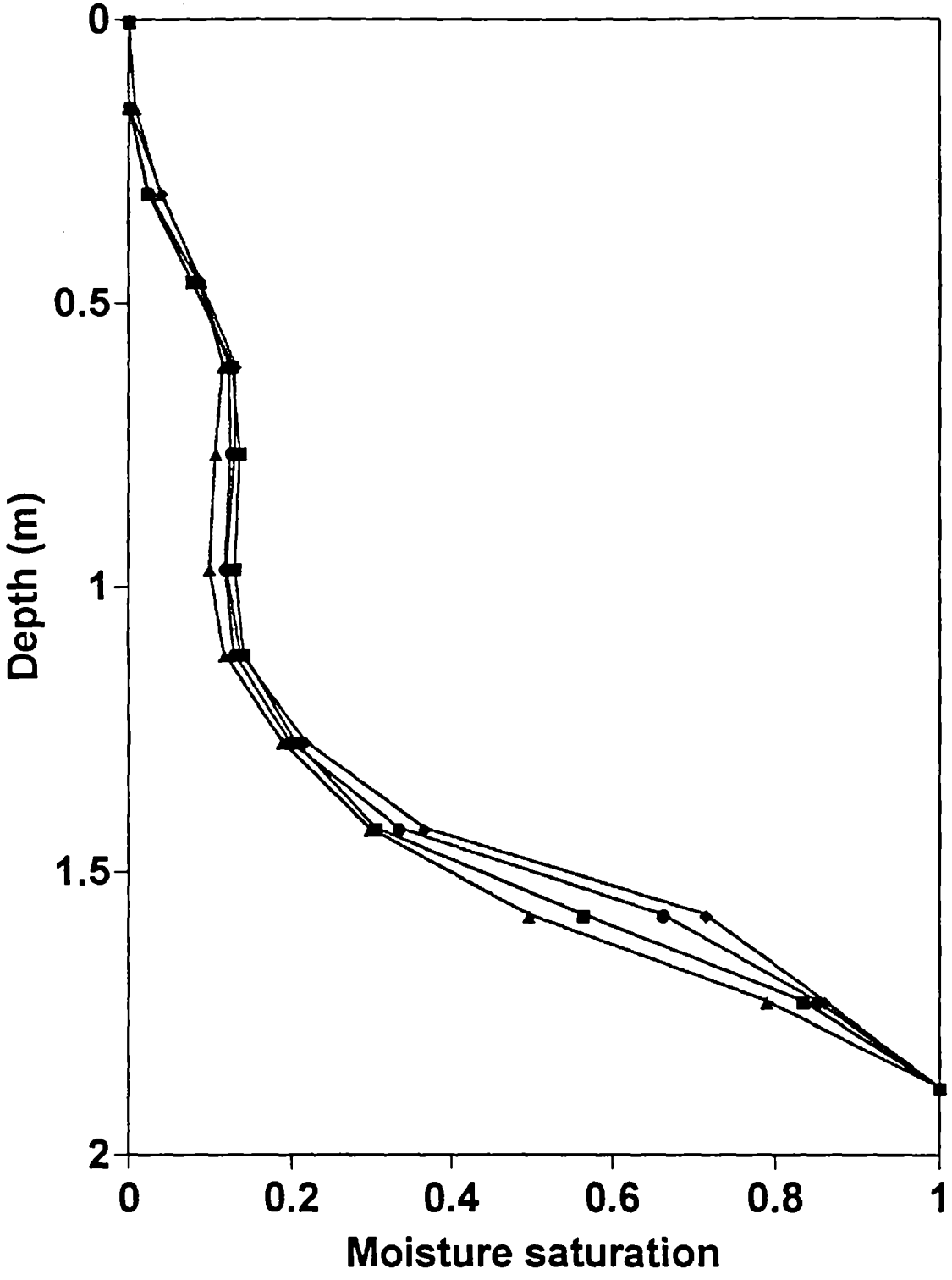

Figure 1. Moisture profiles for the soil-gas chamber

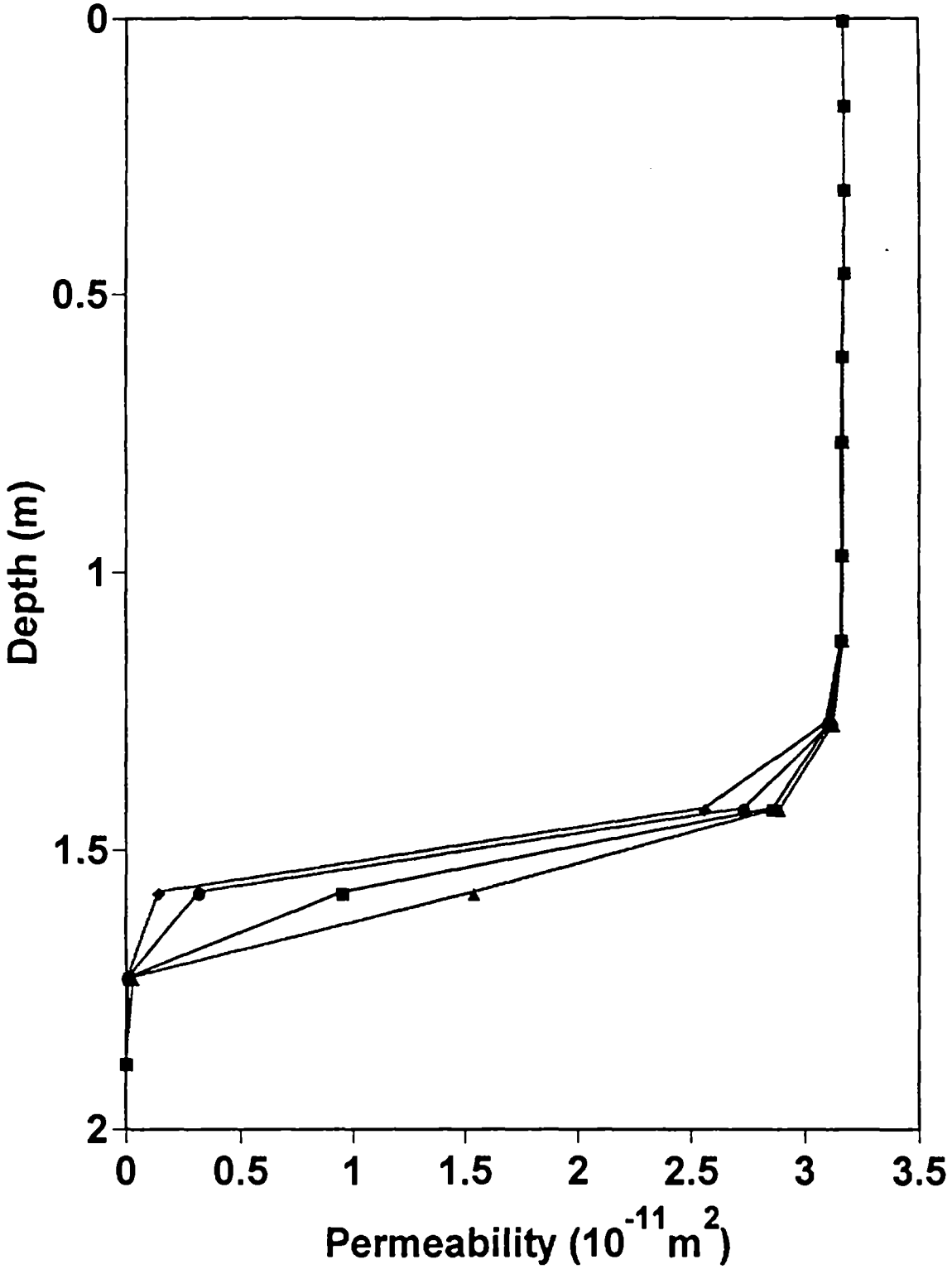

Figure 2. Permeability profiles for the soil-gas chamber

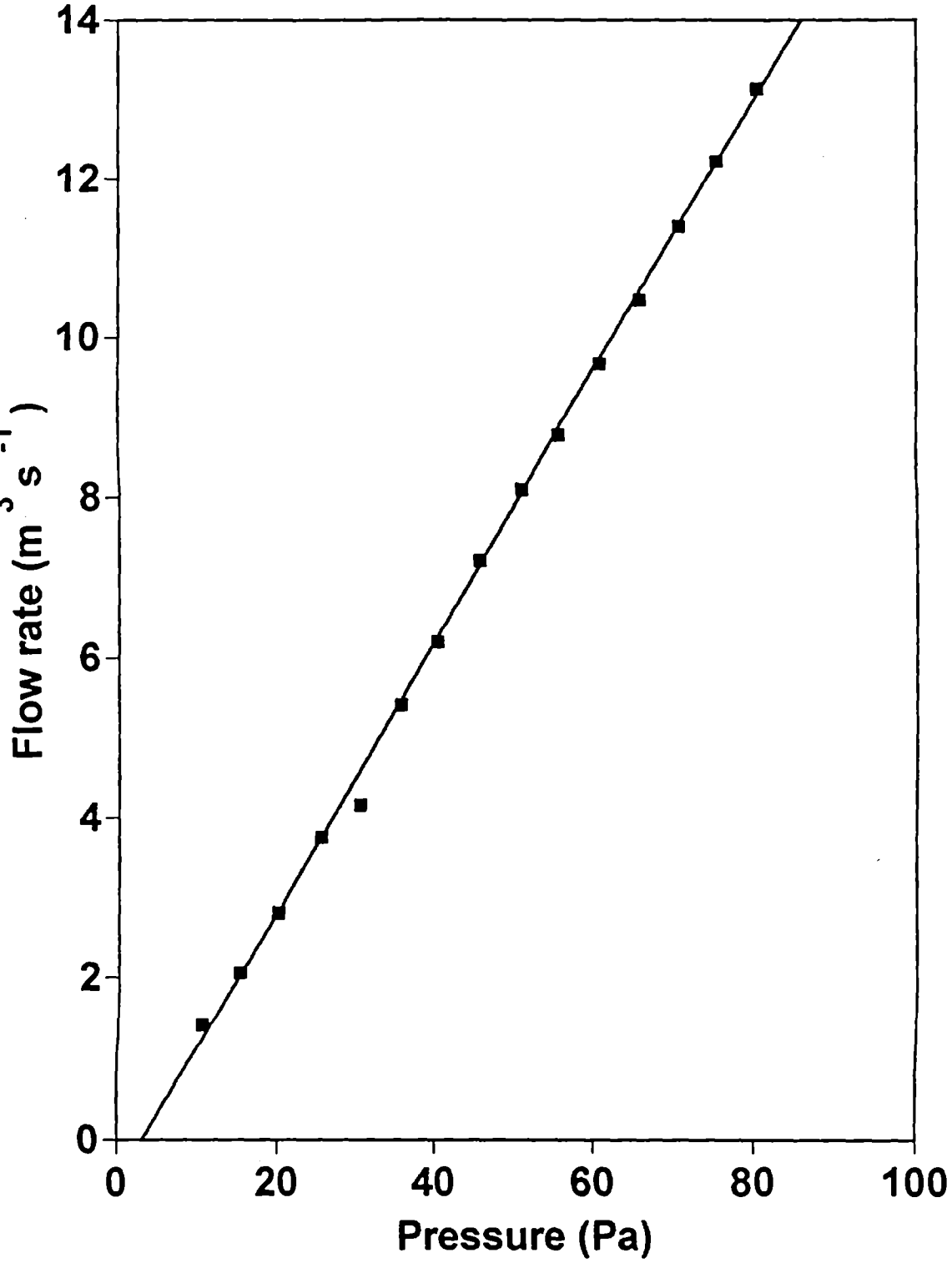

Figure 3. Plot of the total flow/pressure relationship.

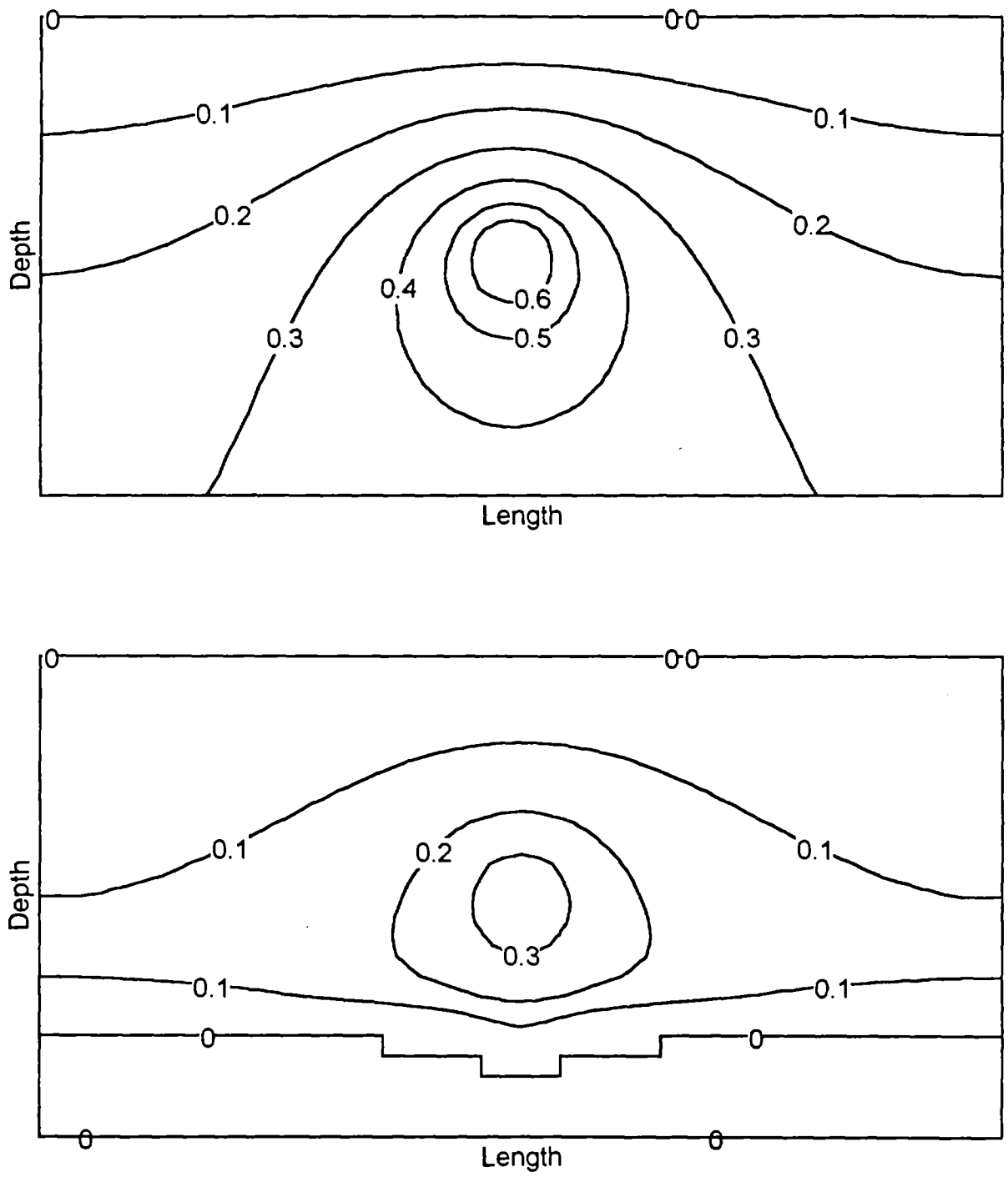

Figure 4. Pressure contours for the soil-gas chamber. The top corresponds to constant permeability, and the bottom corresponds to variable permeability.

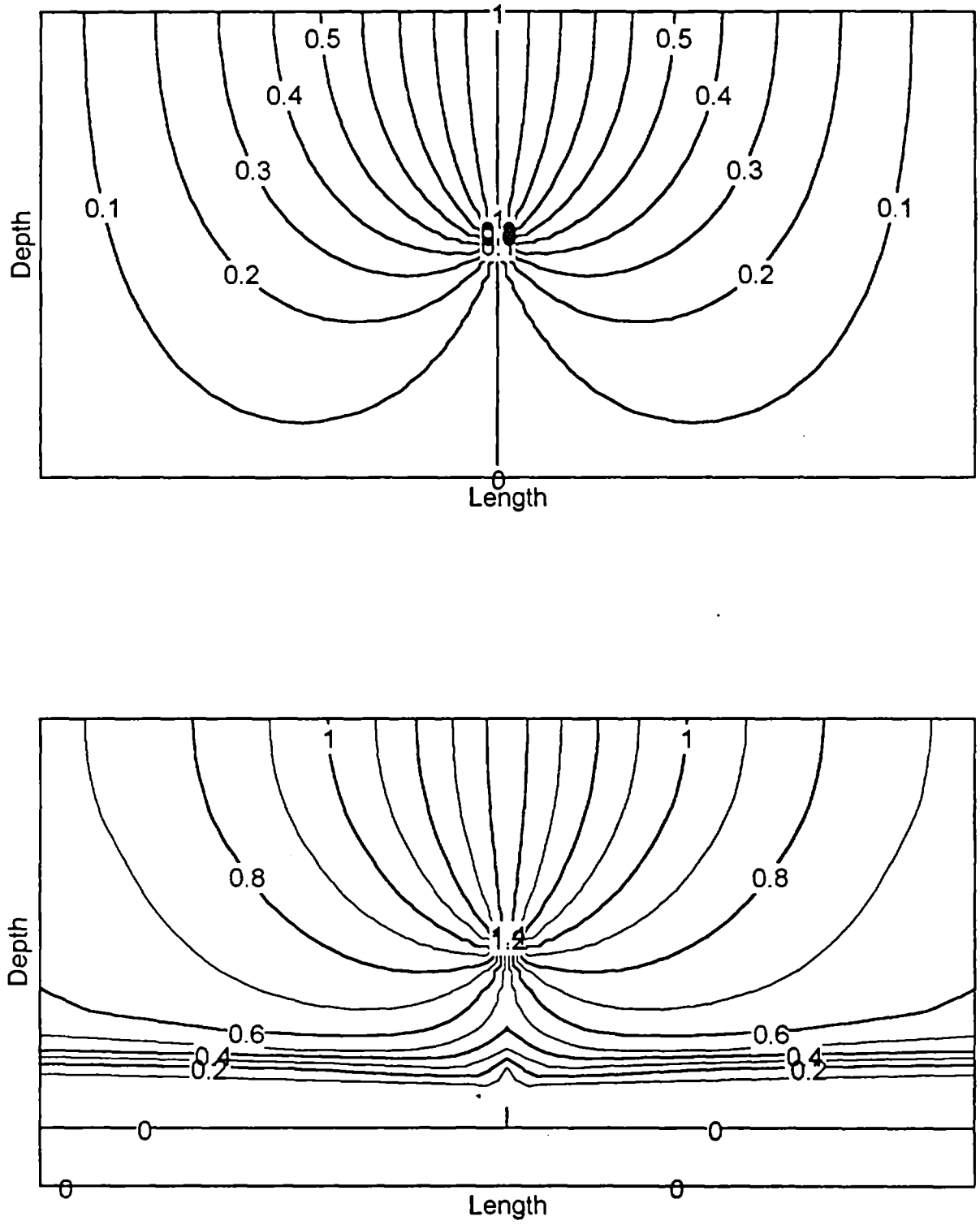

Figure 5. Calculated streamlines for the soil-gas chamber. The top corresponds to constant premeability, and the bottom corresponds to variable permeability.

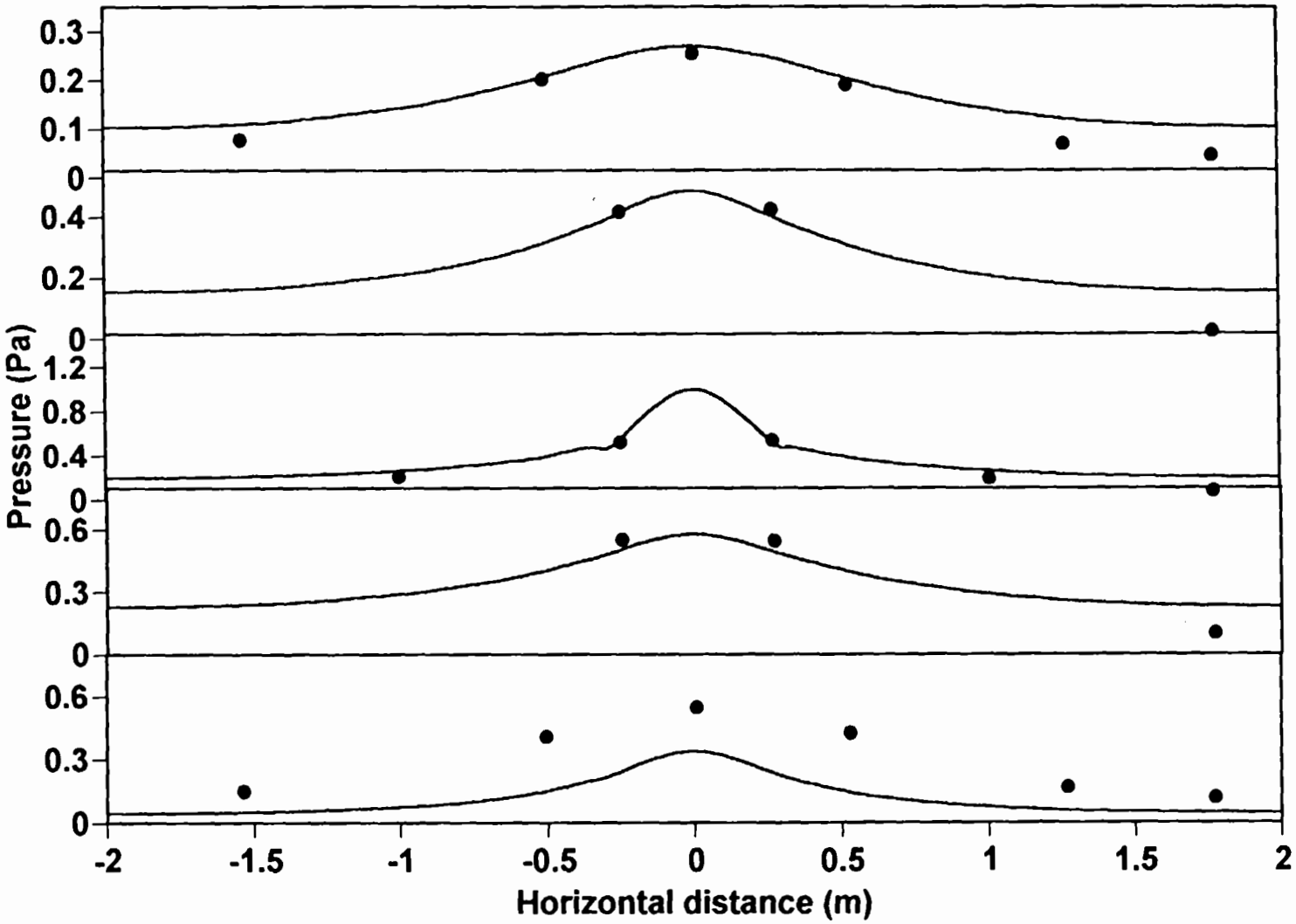

Figure 6. Pressure as a function of horizontal position at five different depths in the soil-gas chamber. Curves represent calculations while symbols represent measurements.

AEERL-P-1110

TECHNICAL REPORT DATA
(Please read Instructions on the reverse before completing)

1. REPORT NO.	2.	3.
EPA/600/A-93/253		

4. TITLE AND SUBTITLE	5. REPORT DATE
Measurements of Soil Permeability and Pressure Fields in EPA's Soil-gas Chamber	6. PERFORMING ORGANIZATION CODE
7. AUTHOR(S)	8. PERFORMING ORGANIZATION REPORT NO.
R. B. Mosley (EPA) and R. Snoddy and S. A. Brubaker Jr. (Acurex)	
9. PERFORMING ORGANIZATION NAME AND ADDRESS	10. PROGRAM ELEMENT NO.
Acurex Corporation P. O. Box 13109 Research Triangle Park, North Carolina 27709	11. CONTRACT/GRANT NO. 68-D2-0063, Task 1/023
12. SPONSORING AGENCY NAME AND ADDRESS	13. TYPE OF REPORT AND PERIOD COVERED
EPA, Office of Research and Development Air and Energy Engineering Research Laboratory Research Triangle Park, NC 27711	Published paper; 5-8/93 14. SPONSORING AGENCY CODE EPA/600/13

15. SUPPLEMENTARY NOTES AEERL project officer is Ronald B. Mosley, Mail Drop 54, 919/541-7865. Presented at 1993 International Radon Conference, Denver, CO, 9/20-23/93.

16. ABSTRACT The paper discusses the measurement of soil permeability and pressure fields using EPA's soil-gas chamber, designed to study the production and transport of radon and other potential indoor air pollutants originating in soils. The chamber is instrumented to measure distributions of radon and pressure fields and also moisture distributions and their resulting influence on soil permeability. An analytic solution for advective flow in the soil-gas chamber is presented which includes the effects of moisture-dependent variations of the permeability with position. Measurements of the pressure field are compared with model calculations. Relatively good agreement between the measurements and calculations is obtained, except near the water level where boundary conditions are not rigorously satisfied.

17. KEY WORDS AND DOCUMENT ANALYSIS

a. DESCRIPTORS		b. IDENTIFIERS/OPEN ENDED TERMS	c. COSATI Field/Group
Pollution	Pressure Field Detection	Pollution Control	13B
Radon		Stationary Sources	07B 17K
Measurement	Moisture		14G 07D
Soils	Mathematical Models		08G, 08M 12A
Permeability			
Test Chambers			14B

18. DISTRIBUTION STATEMENT	19. SECURITY CLASS (This Report)	21. NO. OF PAGES
Release to Public	Unclassified	
	20. SECURITY CLASS (This page) Unclassified	22. PRICE

EPA Form 2220-1 (9-73)